

On the astrophysical robustness of neutron star merger r-process

O. Korobkin^{1*}, S. Rosswog^{1,2,3,†}, A. Arcones^{4,5,‡} C. Winteler^{6,§}

¹*School of Engineering and Science, Jacobs University Bremen, Germany*

²*TASC, Department of Astronomy and Astrophysics, University of California, Santa Cruz, CA 95064, USA*

³*Astronomy and Oskar Klein Centre, Stockholm University, AlbaNova, SE-10691 Stockholm, Sweden*

⁴*Institut für Kernphysik, Technische Universität Darmstadt, Schlossgartenstraße 2, D-64289 Darmstadt, Germany*

⁵*GSI Helmholtzzentrum für Schwerionenforschung GmbH, Planckstr. 1 D-64291 Darmstadt, Germany*

⁶*Department of Physics, University Basel, Switzerland*

Accepted 2012. Received 2012; in original form 2012

ABSTRACT

In this study we explore the nucleosynthesis in the dynamic ejecta of compact binary mergers. We are particularly interested in the question how sensitive the resulting abundance patterns are to the parameters of the merging system. Therefore, we systematically investigate combinations of neutron star masses in the range from 1.0 to 2.0 M_{\odot} and, for completeness, we compare the results with those from two simulations of a neutron star black hole merger. The ejecta masses vary by a factor of five for the studied systems, but all amounts are (within the uncertainties of the merger rates) compatible with being a major source of cosmic r-process. The ejecta undergo a robust r-process nucleosynthesis which produces all the elements from the second to the third peak in close-to-solar ratios. Most strikingly, this r-process is extremely robust, all 23 investigated binary systems yield practically identical abundance patterns. This is mainly the result of the ejecta being extremely neutron rich ($Y_e \approx 0.04$) and the r-process path meandering along the neutron drip line so that the abundances are determined entirely by nuclear rather than by astrophysical properties. While further questions related to galactic chemical evolution need to be explored in future studies, we consider this robustness together with the ease with which both the second and third peak are reproduced as strong indications that compact binary mergers are prime candidates for the sources of the observed unique heavy r-process component.

Key words: neutrinos – nuclear reactions, nucleosynthesis, abundances

1 INTRODUCTION

About half of the elements heavier than iron are formed by neutron capture reactions that occur rapidly in comparison with β -decays. The basic physical mechanisms of this “rapid neutron capture” or “r-process”, for short, had been identified already in the seminal paper of Burbidge et al. (1957). Nevertheless, the cosmic cauldrons in which these heavy elements are forged have remained elusive for more than half a century. Observations of metal-poor stars point to at least two groups of r-process events. The first one is rare and produces whenever it occurs the heaviest r-process elements in nearly exactly solar proportions. The second one, occurs more frequently and produces predomi-

nantly lighter elements from strontium to silver (Cowan & Sneden 2006; Honda et al. 2006). Given that its signature is less unique the second component might also be the result of a superposition from several sources (see e.g. Arcones & Montes (2011); Frischknecht et al. (2012)). Metal-poor stars that are enriched by r-process material show patterns that very closely match the (scaled) solar system abundances for nuclei beyond Ba ($Z=56$). This suggests that this heavy r-process component is produced only if a very unique set of astrophysical conditions is realized, or, alternatively, that it is produced in a range of realizations, but is insensitive to the exact parameters of its formation environment. So far, there is no generally accepted explanation for the unique heavy r-process component.

Historically supernovae were considered the “natural” source of r-process elements, but this view has recently been distressed by a slew of investigations (e.g. Arcones et al. (2007); Roberts et al. (2010); Fischer et al. (2010); Hudepohl

* E-mail: o.korobkin@jacobs-university.de

† E-mail: s.rosswog@jacobs-university.de

‡ E-mail: almudena.arcones@physik.tu-darmstadt.de

§ E-mail: christian.winteler@unibas.ch

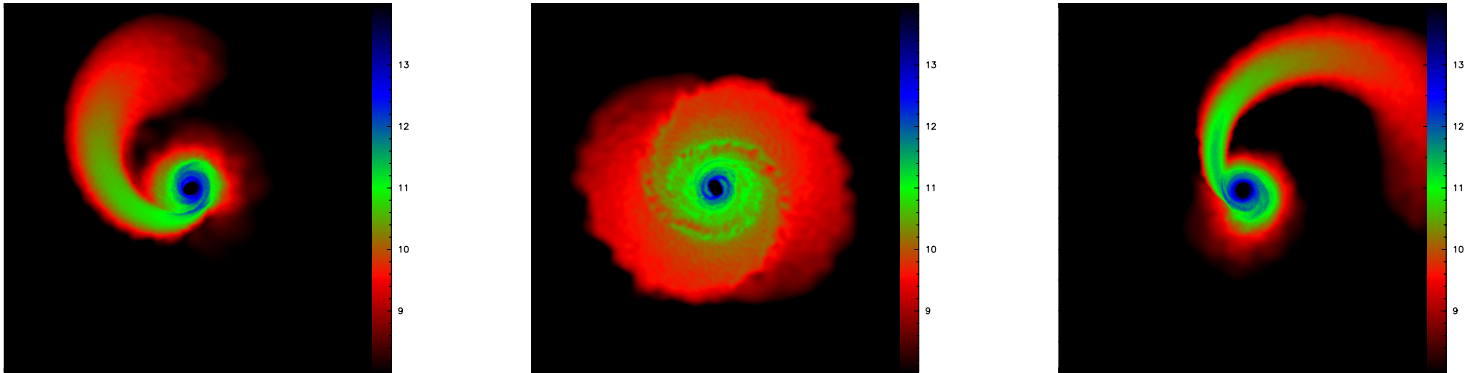


Figure 1. Sensitivity to mass ratio: shown are density cuts ($[600 \text{ km} \times 600 \text{ km}]$, colour-coded is the logarithm of density in cgs units) of a $1.2\text{-}1.4 M_{\odot}$ ($t = 13.9 \text{ ms}$), a $1.4\text{-}1.4 M_{\odot}$ ($t = 13.4 \text{ ms}$) and a $2.0\text{-}1.4 M_{\odot}$ ($t = 15.0 \text{ ms}$) merger.

et al. (2010)). These studies found neutrino-driven winds in supernovae to be seriously challenged in providing the physical conditions (high entropy, low electron fraction together with rapid expansion) that are required to produce the heavy ($A > 90$) r-process elements. A possible exception may be magnetorotationally driven supernova jets where the fast ejection of highly compressed neutron-rich matter produces interestingly low electron fraction values (Winteler et al. 2012). It remains to be explored, however, how robust this scenario is with respect to the stellar parameters and with respect to its nucleosynthetic yields. The main contenders of supernovae in terms of r-process nucleosynthesis are compact binary mergers of either two neutron stars (ns^2) or a neutron star and a stellar-mass black hole (nsbh) (Lattimer & Schramm 1974, 1976; Eichler et al. 1989; Freiburghaus et al. 1999).

Since the first nucleosynthesis calculations for neutron star merger ejecta (Freiburghaus et al. 1999) have been performed, numerical models have seen vast improvements in physics, numerical methods and resolution and we consider it timely to address this important topic again. There have been recent r-process studies in a compact binary merger context (Roberts et al. 2011; Goriely et al. 2011; Wanajo & Janka 2012) which, in agreement with the results of the first study, confirm the occurrence of a robust r-process. While all previous studies provided new insights each of them had its limitations. For example, in all of them the ejecta electron fraction was poorly known since Y_e -changing weak interactions were ignored. More importantly, the ns^2 parameter space was explored only very punctually around ns masses of $1.4 M_{\odot}$ (Freiburghaus et al. (1999) explored one case from Rosswog et al. (1999), two cases were explored in the conformal flatness approximation approach of Goriely et al. (2011)¹ and three cases in Roberts et al. (2011)). In recent years, however, it has become clear that the neutron stars realized in nature span a substantial range in masses, see e.g. Lattimer & Prakash (2010) for compilation of neutron star masses. Therefore, an important open question needs to be answered: “How sensitive is the compact object

merger nucleosynthesis to the actual astrophysical system that merges?”

This is what we address in this paper: we systematically scan the neutron star binary parameter space in 21 simulations and we calculate the resulting nucleosynthetic products. For completeness, we also show the results for the ejecta of two nsbh systems. Apart from exploring a very large neutron star mass range, we also significantly improve on the treatment of the electron fraction Y_e : we start with cold neutron stars in β -equilibrium and allow for the evolution of Y_e via electron and positron captures (Rosswog & Liebendörfer 2003). We demonstrate that the nucleosynthesis results are essentially independent of the parameters of merging system, i.e. every ns^2 or nsbh system produces nearly exactly the same abundance pattern. The results show, however, some sensitivity to the properties of extremely neutron-rich nuclei (e.g. binding energy, half-lives, fission properties) which are not well known (Thielemann et al. 2011).

Although heavy element nucleosynthesis is the clear focus of this study, we would like to stress the importance of compact object merger ejecta and their nucleosynthesis in a broader astrophysical perspective. Both the LIGO and Virgo gravitational wave (GW) detectors are currently being upgraded (Abbott et al. 2009; Smith 2009; Sengupta et al. 2010) to a $\sim 10 - 15$ times better sensitivity than the original versions of the instruments. This will increase the volume of accessible astrophysical sources by more than a factor of 1000 reaching a detection horizon of a few hundred Mpc for ns^2 mergers and about a Gpc for nsbh mergers (Abadie et al. 2010). Since the first detections will most likely be around or even below threshold it is of paramount importance to identify accompanying electromagnetic signatures of the most promising GW sources to enhance the confidence in a possible detection. Short gamma-ray bursts are likely the brightest electromagnetic manifestations that result from a compact binary merger, but also the r-process nucleosynthesis and the decay of the resulting radioactive nuclei may leave an observable signature as optical/UV transients, so-called “macronovae” (Li & Paczyński 1998; Kulkarni 2005; Rosswog 2005; Metzger et al. 2010; Roberts et al. 2011; Metzger & Berger 2012). For neutron star mergers they are expected to peak about 10 hours after the mergers with a few times

¹ These authors also used the Lattimer-Swesty EOS to test for the impact of the neutron star equation of state.

10^{42} erg/s (Rosswog et al. 2012; Piran et al. 2012). Later, on time scales of months to years, the ejecta dissipate their kinetic energy in the ambient medium and thereby produce possibly detectable radio flares (Nakar & Piran 2011; Piran et al. 2012).

This paper is structured as follows. In Sec. 2 we briefly summarize our simulations and explore the amount of ejected matter as a function of the binary system parameters. In Sec. 3 we describe how we calculate the nuclear abundances and we discuss how they depend on the astrophysical properties of the merging system and on the nuclear physics input. In Sec. 4 we summarize our results and discuss their astrophysical implications.

2 HYDRODYNAMIC EVOLUTION AND DYNAMICALLY EJECTED MASS

2.1 Explored parameter space

Until recently, the neutron star mass distribution was thought to be clustered narrowly around $1.35 M_{\odot}$ (Thorsett & Chakrabarti 1999). Therefore, essentially all neutron star merger studies have focused on a narrow range of masses around this value. Recent observations, however, indicate a much broader neutron star mass spectrum. There is now ample support for neutron star masses significantly larger than $1.5 M_{\odot}$. A broad peak around 1.5 - $1.7 M_{\odot}$ has been found (Kiziltan et al. 2010; Valentim et al. 2011) for neutron stars with white dwarf companions, an additional low-mass peak near $1.25 M_{\odot}$ is thought to be characteristic for neutron stars that were produced by electron capture supernovae (Podsiadlowski et al. 2004; van den Heuvel 2004; Schwab et al. 2010). PSR J1614-2230 with $1.97 \pm 0.04 M_{\odot}$ possesses the largest accurately known neutron star mass (Demorest et al. 2010), but even higher masses may exist in nature. For example, the mass of the black widow pulsar has recently been determined as $2.4 \pm 0.12 M_{\odot}$ (van Kerkwijk et al. 2011). On the lower mass side, the secondary neutron star in J1518+4904 has a best estimated mass value of only $0.72 M_{\odot}$, although with a very large 1σ error bar of $0.5 M_{\odot}$, see Lattimer & Prakash (2010) and references therein.

We take these results as a motivation for a systematic exploration of the parameter space from 1.0 to $2.0 M_{\odot}$ in steps of $0.2 M_{\odot}$. Since the neutron star viscosity cannot substantially spin up the neutron stars during the short tidal interaction phase preceding the merger (Bildsten & Cutler 1992; Kochanek 1992) all our models have vanishing initial ns spins. Our ns² cases are complemented by two nsbh cases with black hole masses of 5 and $10 M_{\odot}$, for an overview over the performed simulations see Tab. 1.

2.2 Methodology

To follow the hydrodynamic evolution we use the Smooth Particle Hydrodynamics (SPH) method, see Monaghan (2005) and Rosswog (2009) for recent reviews, which, due to its completely Lagrangian nature, is ideally suited to follow the ejected material. Our code is an updated version of the one that was used in earlier studies (Rosswog & Davies 2002; Rosswog & Liebendörfer 2003; Rosswog et al. 2003; Rosswog 2005). It uses the Shen et al. equation of state (EOS) (Shen

et al. 1998a,b) and an opacity-dependent multi-flavour neutrino leakage scheme (Rosswog & Liebendörfer 2003). The latter allows in particular to follow the Y_e -changes due to electron and positron captures. Moreover, we use a modern, time-dependent artificial viscosity prescription, see Rosswog et al. (2000, 2008) for details. The presented calculations make use of Newtonian gravity which leads to less compact neutron stars than General Relativity. This could have a moderate effect on the amount of ejecta mass and, since the β -equilibrium Y_e is determined by the density inside the initial neutron star, the electron fraction. As we will show below, however, the heavy nucleosynthesis is only affected once Y_e reaches ~ 0.2 and the ejecta masses are (within the existing uncertainties) still consistent with compact binary mergers being a major *r*-process source even if the amount of ejecta is reduced by a factor of a few. Therefore, we expect our major results to be robust. Nevertheless this point needs improvement in future work.

2.3 Ejecta properties

The merger dynamics is rather sensitive to asymmetries in the component masses, see Fig. 1 (for a more complete overview over the remnant structures see Fig. 1 in Piran et al. (2012)). The asymmetries enhance the degree to which the secondary is disrupted and they lead to larger ejecta masses and velocities. As already pointed out by Oechslin et al. (2007), the ejecta stem from two different regions: a hot component from the interaction region between the stars (subsequently called “interaction-” or *i*-component for short) and a colder one where matter is simply flung out by tidal torques, see the first two panels in Fig. 2. We refer to this matter as “tidal” or *t*-component. As the mass ratio decreases, the primary only ejects small amounts of the *i*-component, while the fraction and overall amount in the *t*-component from the secondary increases. This differs from the findings of Goriely et al. (2011), where even in unequal-mass cases most of the mass is lost from the primary as *i*-component. For now we can only speculate about the origin of this difference: it could either be due the different treatment of self-gravity (conformal flatness vs Newtonian) or, since the *i*-component comes from a region of very strong shear, it could also to some extent be impacted by the specifics of numerical method, such as implementation of artificial viscosity.

As can be seen from the volume rendering in panel 3 of Fig. 2, the ejecta are extremely neutron-rich. In Fig. 3, left panel, we bin the mass fractions of the ejecta of all simulations according to Y_e . The values are clustered around $Y_e = 0.03$ and dominated by *t*-component material. Since at high densities the Y_e -changing reactions are Pauli-blocked and the subsequent rapid expansion leads to a very fast temperature drop, the *t*-component had essentially no time to change its electron fraction. Therefore, it still carries the original Y_e -value set by cold, high-density β -equilibrium inside the neutron star. The Y_e of this matter therefore is a unique function of density which shows up as well-defined curve in the inset of Fig. 3. The scattered component in this inset is a combination of matter from the *i*-region and matter from the high Y_e neutron star crust which is only marginally resolved in our simulations. The *t*-component of the ejecta not only starts within a narrow range of thermodynamical

Table 1. Overview over the performed simulations, the superscript ⁺ indicates that the primary is a black hole.

Run	m_1 [M_\odot]	m_2 [M_\odot]	N_{SPH} [10^6]	t_{end} [ms]	m_{ej} [M_\odot]	comment
1	1.0	1.0	1.0	15.3	7.64×10^{-3}	
2	1.2	1.0	1.0	15.3	2.50×10^{-2}	
3	1.4	1.0	1.0	16.5	2.91×10^{-2}	
4	1.6	1.0	1.0	31.3	3.06×10^{-2}	
5	1.8	1.0	1.0	30.4	$> 1.64 \times 10^{-2}$	secondary still orbiting
6	2.0	1.0	0.6	18.8	$> 2.39 \times 10^{-2}$	secondary still orbiting
7	1.2	1.2	1.0	15.4	1.68×10^{-2}	
8	1.4	1.2	1.0	13.9	2.12×10^{-2}	
9	1.6	1.2	1.0	14.8	3.33×10^{-2}	
10	1.8	1.2	1.0	21.4	3.44×10^{-2}	
11	2.0	1.2	0.6	15.1	$> 2.95 \times 10^{-2}$	secondary still orbiting
12	1.4	1.4	1.0	13.4	1.28×10^{-2}	
13	1.6	1.4	1.0	12.2	2.36×10^{-2}	
14	1.8	1.4	1.0	13.1	3.84×10^{-2}	
15	2.0	1.4	0.6	15.0	3.89×10^{-2}	
16	1.6	1.6	1.0	13.2	1.97×10^{-2}	
17	1.8	1.6	1.0	13.0	1.67×10^{-2}	
18	2.0	1.6	0.6	12.4	3.79×10^{-2}	
19	1.8	1.8	1.0	14.0	1.50×10^{-2}	
20	2.0	1.8	0.6	11.0	1.99×10^{-2}	
21	2.0	2.0	0.2	21.4	1.15×10^{-2}	
22	5.0 ⁺	1.4	0.2	138.7	2.38×10^{-2}	nsbh
23	10.0 ⁺	1.4	0.2	139.0	4.93×10^{-2}	nsbh

parameters, $Y_e = 0.04 \pm 0.02$, $\rho = (1.4 \pm 0.5) \times 10^{14} \text{ g cm}^{-3}$, corresponding to the outer ~ 2 km of the original neutron star (see, for example, Fig. 1 in Rosswog et al. (2012)), but also continues to expand adiabatically and without shocks. Therefore, all fluid elements in tidal ejecta share approximately the same thermodynamic history and provide robust conditions for a uniform nucleosynthesis.

The amounts of ejected matter range from 7.6×10^{-3} to $3.9 \times 10^{-2} M_\odot$ ($4.9 \times 10^{-2} M_\odot$ in the nsbh case). We see a clear trend for decreasing mass ratios to eject more matter, but for the equal-mass systems no unique trend is found with respect to the total binary mass. For at least small ns mass asymmetries, i.e. for the most common cases, we provide a fit formula based on the dimensionless mass asymmetry parameter

$$\eta := 1 - 4m_1m_2/(m_1 + m_2)^2. \quad (1)$$

Contrary to the mass ratio q , η is symmetric with respect to both masses and varies only in a finite range from 0 to 1 (with 0 for an equal-mass system and η approaching 1 for

extreme mass ratios)². The fit formula

$$m_{\text{ej}}(m_1, m_2) = (m_1 + m_2) \left(A - B\eta - \frac{C}{1 + \eta^3/\sigma^3} \right), \quad (2)$$

with $A = 0.0125$, $B = 0.015$, $C = 0.0083$ and $\sigma = 0.0056$, shown as solid line in Fig. 3, right panel, provides a reasonably good approximation to the simulation results. For unequal-mass binaries $m_{\text{ej}}/(m_1 + m_2)$ tends to a minimum when approaching $\eta \rightarrow 0$ and a maximum of ≈ 0.12 is reached near $\eta = 0.02$.

3 NUCLEOSYNTHESIS

3.1 Hydrodynamic trajectories

Our nucleosynthesis calculations are performed with a large reaction network (Winteler 2012; Winteler et al. 2012) that is based on the BasNet network (Thielemann et al. 2011). It includes over 5800 isotopes from nucleons up to $Z = 111$ between the neutron drip line and stability. The reaction rates are from the compilation of Rauscher & Thielemann (2000)

² A similar parameter $\bar{\eta} = m_1m_2/(m_1 + m_2)^2$ was used in deriving an empirical formula for recoil velocities of coalescing non-spinning black holes (González et al. 2007; Fitchett 1983)

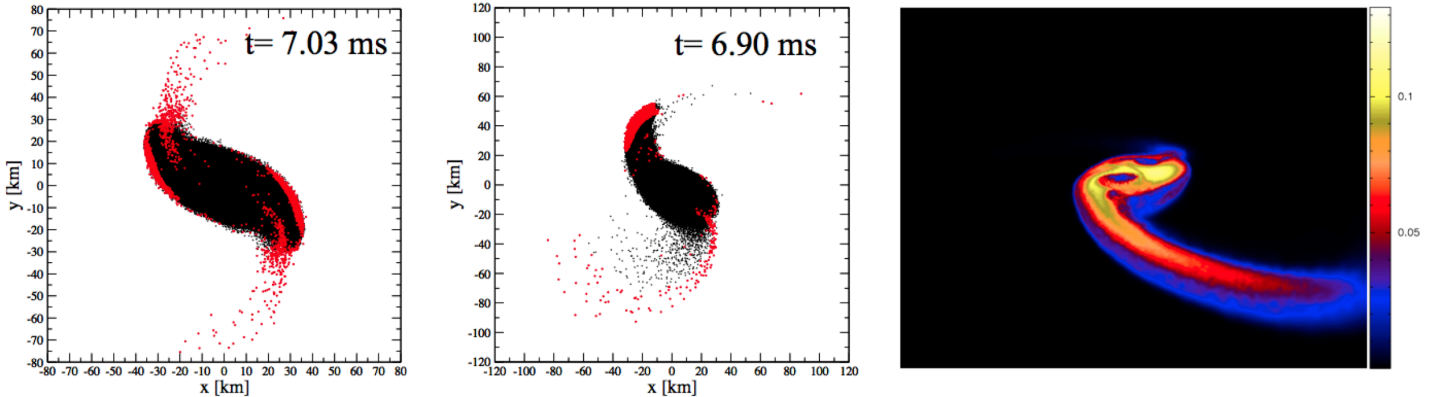


Figure 2. The ejecta come from two different regions (left and middle): a hot interaction region between the stars where matter is ejected by hydrodynamic effects and a colder region that is flung out by tidal torques. The fraction of the latter material increases with the asymmetry in the stellar masses (left $1.4 + 1.4 M_{\odot}$, right $1.8 + 1.4 M_{\odot}$). Right: volume rendering of the Y_e distribution ($1.4 + 1.2 M_{\odot}$ at $t = 8.09$ ms), only matter below the orbital plane is shown.

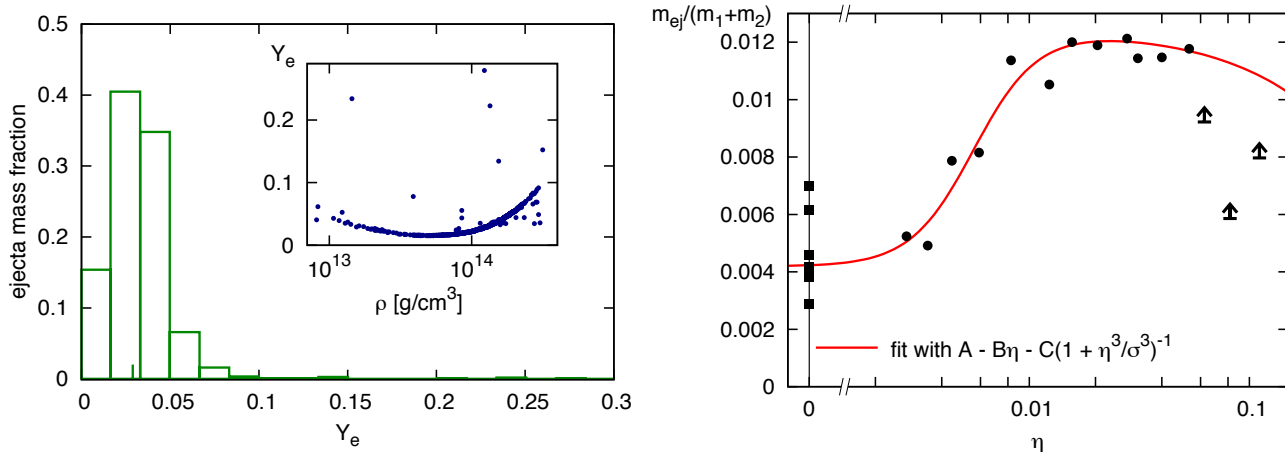


Figure 3. Left panel: Distribution of Y_e in the selected subset of ejected particles in all ns^2 and $nsbh$ simulations, binned by mass. The inset shows how Y_e is correlated with the initial density in each particle before the merger. Majority of points on the Y_e - ρ diagram trace the neutron star composition in the layer below the crust, where the $Y_e(\rho)$ reaches minimum. As a consequence, Y_e in the ejecta is narrowly distributed around $Y_e \sim 0.04$. Right panel: Fit of the ejected mass normalized by the total mass of the binary as a function of the asymmetry parameter η (see main text for definition). Coefficients of the fit are: $A = 0.0125$, $B = 0.015$, $C = 0.0083$, and $\sigma = 0.0056$. The arrows indicate the lower limits on the ejected mass for the three simulations in which the secondary is still not fully disrupted.

for the finite range droplet model (FRDM) (Möller et al. 1995) and the weak interaction rates (electron/positron captures and β -decays) are the same as in Arcones & Martinez-Pinedo (2011). In addition, neutron capture and neutron-induced fission rates of Panov et al. (2010) and β -delayed fission probabilities as described in Panov et al. (2005) are used.

The thermodynamical conditions are taken from hydrodynamical trajectories of individual SPH particles. We calculate nucleosynthetic yields for 30 representative trajectories in each of the 21 ns^2 merger simulations, and for 20 trajectories in the two $nsbh$ merger simulations. These trajectories are a fair representation of the total ejected mass, see Tab. 1. Once matter has been ejected from the central high-density

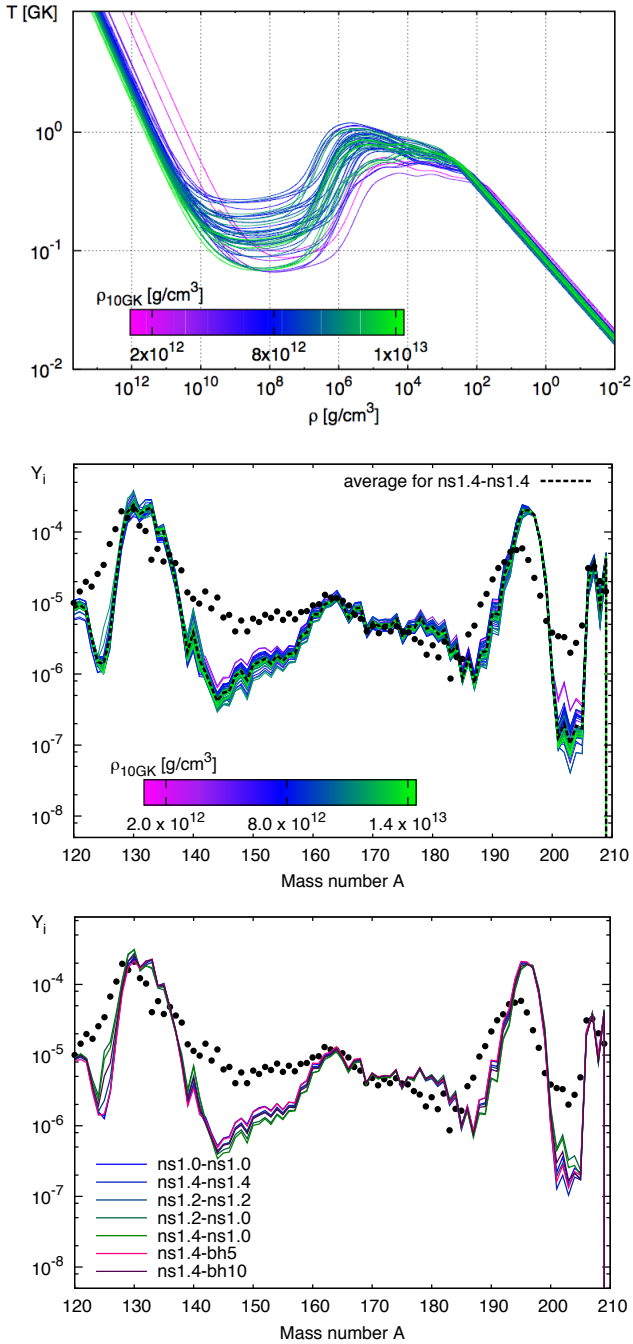


Figure 4. Top: density and temperature evolution for a bundle of trajectories, color-coded by density at $T = 10$ GK. Middle: resulting final abundances distribution. Their averaged distribution is shown in a black dashed line, and a bold red line represents abundances for a trajectory without heating. All trajectories represent a subset from the standard $1.4\text{-}1.4 M_{\odot}$ merger. Bottom: distribution of abundances for a variety of different (ns² and nsbh) merger cases. All different astrophysical systems yield essentially identical resulting abundances.

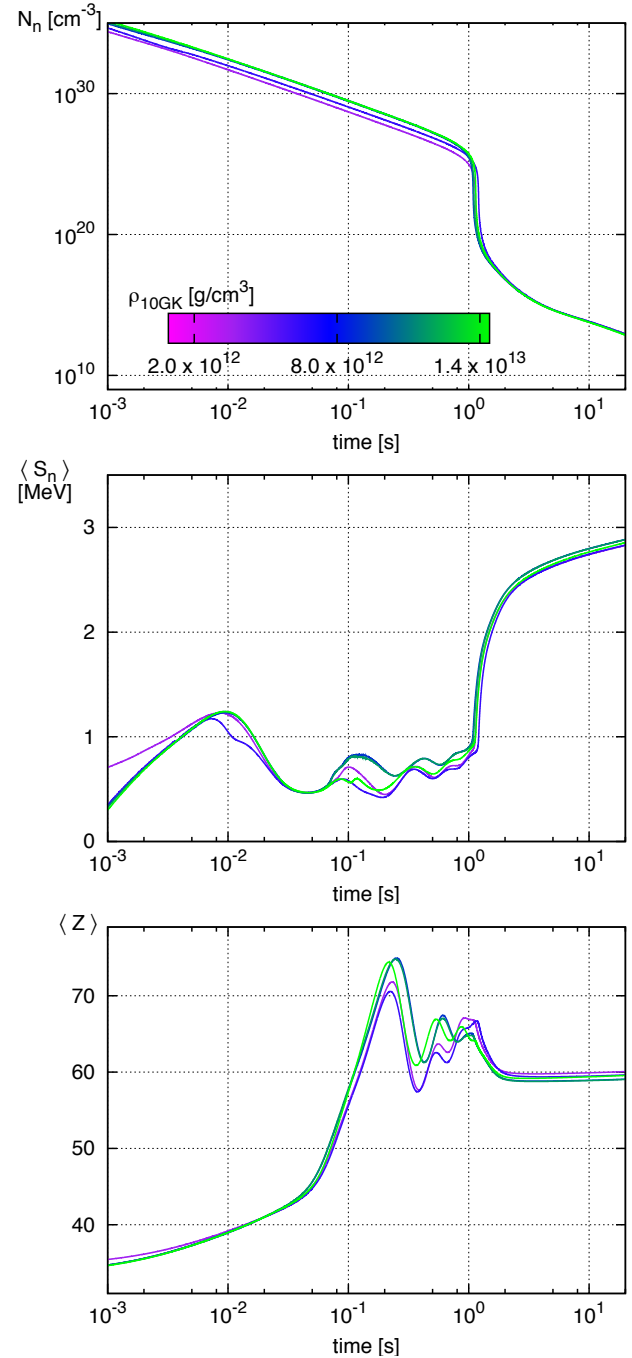


Figure 5. Evolution of the neutron density N_n (top), average neutron separation energy $\langle S_n \rangle$ (middle) and average proton number $\langle Z \rangle$ (bottom) for five trajectories from run 12 with different initial densities (in the range $10^{12} - 10^{13} \text{ g}/\text{cm}^3$).

region, both temperature and density decrease rapidly while the electron fraction Y_e can, in principle, start to increase due to β -decays and positron captures. A small fraction of the trajectories (less than 0.008, see Fig. 3, left panel) suffers shocks during their later evolution during which their Y_e increases up to ~ 0.25 , but for the bulk of trajectories the Y_e -values remain essentially constant. Some of the higher Y_e -material also comes from the (marginally resolved) neutron star crust material. Although heavily dominated by values

around 0.03, our ejecta electron fractions show a broader range than those of Goriely et al. (2011), probably due to our higher resolution (crust material) and their omission of weak interactions.

We start our nucleosynthesis calculations when the temperature of the trajectory has dropped below $T_0 = 10$ GK. The initial composition is given by nuclear statistical equilibrium and it is further evolved with the complete network. Because most of the trajectories from hydrodynamical simulations terminate after $t_{\text{fin}} \sim 10 - 20$ ms, we extrapolate according to a free expansion for the density and an adiabatic expansion law for the temperature:

$$\rho(t) = \rho_{\text{fin}} \left(\frac{t}{t_{\text{fin}}} \right)^{-3}, \quad T(t) = T[S_{\text{fin}}, \rho(t), Y_e(t)],$$

where ρ_{fin} and S_{fin} are the density and entropy at t_{fin} , while the temperature is calculated at each point of time from the equation of state (Timmes & Swesty 2000).

Contrary to neutrino-driven winds where the ejecta are dominated by alpha particles and only few seed nuclei participate in the *r*-process, essentially all matter in neutron star mergers undergoes *r*-process. Therefore the *r*-process energy generation is non-negligible and leads to a substantial temperature increase (see e.g., Freiburghaus et al. 1999; Metzger et al. 2010; Goriely et al. 2011) that could affect the late-time evolution (Metzger et al. 2010). We calculate the *r*-process heating in a post processing step and consider its influence on the nucleosynthesis by modifying the temperature. To account for neutrino energy losses associated with β -decays, we introduce a heating efficiency parameter ϵ_{th} which measures the fraction of nuclear power which is retained in the matter. Metzger et al. (2010) argue that this fraction must be $\epsilon_{th} \approx 0.25 - 1$. As a default, we use $\epsilon_{th} = 0.5$, but below we explore how (in)sensitive the results are to this choice. For a given trajectory we take its initial entropy $S_{\text{hyd}}(t)$ and increment it by $\epsilon_{th} S_{\text{nuc}}(t)$, following the prescription of Freiburghaus et al. (1999).

3.2 Final abundances

The *r*-process nucleosynthesis in compact binary mergers is extremely robust, all 23 cases of Tab. 1 deliver essentially identical abundance distributions. We illustrate the origin of this robustness using the reference case of two neutron stars with $1.4 M_{\odot}$ each (run 12 in Table 1). Fig. 4 shows the density and temperature evolution for all trajectories (upper panel) and their final abundances. Between different trajectories of a single run there is only a very small spread in the resulting abundances, although the evolution of temperature is not always the same. The resulting final abundances (sum over all ejecta trajectories for each run) are practically the same for all cases. We show a representative selection of the results from different runs in the bottom panel of Fig. 4. The robustness of the abundances is mainly due to two factors: 1) the *r*-process path always reaches the drip line because of the extremely neutron-rich conditions and 2) there are several fission cycles (similar to what was observed in Goriely et al. 2011). These conditions lead to the evolution of the neutron density shown in Fig. 5, upper panel. The huge values of the neutron density are due to the (narrow range of) very low Y_e -values.

In our calculations the low Y_e results in an initial composition consisting of neutron-rich nuclei ($Z > 20$, on the neutron drip line) and neutrons. Differences with Goriely et al. (2011) in lighter heavy elements are not particularly relevant because these can also be produced in other astrophysical events, and the overall yields of the elements with $A < 120$ that we obtain are much smaller compared to the heavy robust *r*-process elements (similar to Goriely et al. (2011)). Note that the contribution of the high- Y_e trajectories to the final abundances is negligibly small.

In order to understand the evolution of the *r*-process path we monitor the average neutron separation energy (middle panel Fig. 5) defined as

$$\langle S_n \rangle = \frac{\sum_{Z,A} S_n(Z, A) Y(Z, A)}{\sum_{Z,A} Y(Z, A)}, \quad (3)$$

with $S_n(Z, A)$ and $Y(Z, A)$ being the neutron separation energy and abundance of the nucleus (Z, A). The average separation energy decreases when matter moves away from stability and it is, by definition, zero at the neutron drip line. The second panel of Fig. 5 shows that the average separation energy is initially below ≈ 1 MeV, which indicates that the *r*-process path proceeds along the neutron drip line. The average proton number increases to $Z = 40$ at $t \approx 10^{-2}$ s where the neutron separation energy reaches a maximum. This local maximum occurs when the magic number $N = 82$ is overcome. Whenever the *r*-process path reaches a neutron magic number, it moves closer to the line of β -stability (i.e., larger S_n values) by increasing Z without changing N . After the matter flow passes $N = 82$ (here around $Z = 40$), the $\langle S_n \rangle$ decreases because the path gets again further away from the β -stable region. This continues until the next magic number, $N = 126$, is encountered (corresponding to the minimum of $\langle S_n \rangle$ between 0.01s and 0.1s). Around $t = 0.1$ s and $Z = 60$, $N = 126$ is also overcome as indicated by the second maximum of $\langle S_n \rangle$. After this point the oscillations in $\langle S_n \rangle$ are due mainly to fission as can be seen by the behavior of $\langle Z \rangle$. Note that FRDM predicts a magic number at $N = 184$, consequently the path reaching this point may lead to oscillations in $\langle S_n \rangle$. Therefore, the quantity $\langle Z \rangle$ is a nuclear fission indicator that is better suited than the average mass number (Goriely et al. 2011), since it can decrease only through fission reactions, while the average mass number can also decrease due to photo-dissociations. The maximum $\langle Z \rangle$ corresponds to the moment when a significant amount of matter has reached the region where fission becomes important. The daughter nuclei resulting from fission capture neutrons move first towards the drip line and then to higher Z where fission acts again. In that way several fission cycles occur and lead to oscillations in $\langle Z \rangle$. In Fig. 5 one can distinguish at least three fission cycles. The final increase of $\langle S_n \rangle$ is due to the *r*-process freeze-out at $t \approx 1$ s when the neutron-to-seed ratio drops below unity and the matter β -decays to stability. We have used our reference case of two $1.4 M_{\odot}$ neutron stars, run 12, for illustration purposes, but behaviour is very similar in all of the other cases.

The major result of this study is that the *r*-process abundances for compact binary mergers do not depend on the astrophysical parameters of the merging system. They do depend, however, on the not-so-well-known properties of nuclei close to the neutron drip line. The most critical inputs

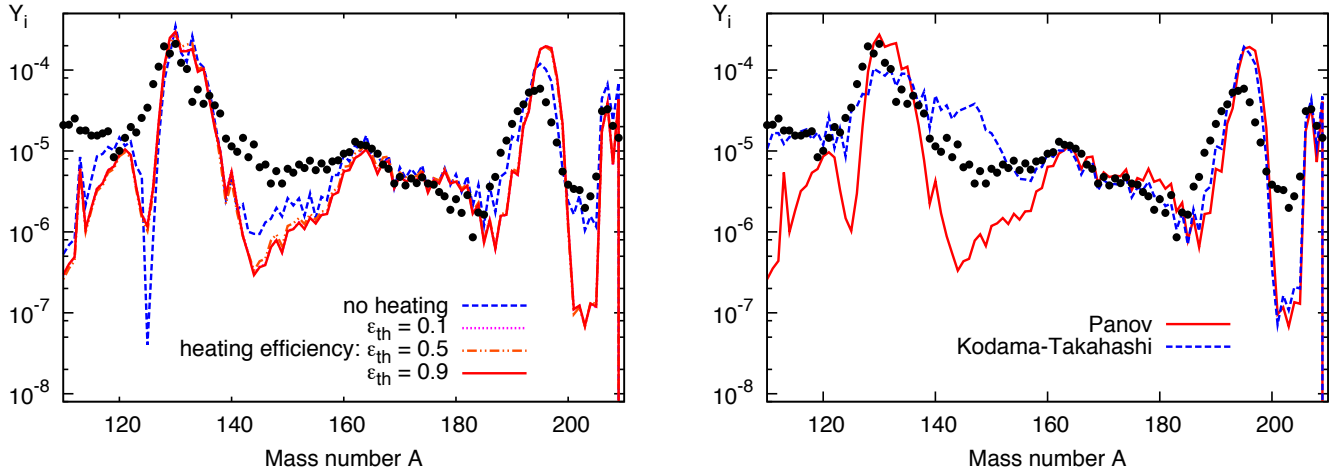


Figure 6. Distribution of final abundances in the vicinity of the second and third r-process peaks. Left: for the case without heating and for three different values of an heating efficiency ϵ_{th} ; Right: for two types of fission fragments mass distribution. Overplotted black dots represent solar abundances.

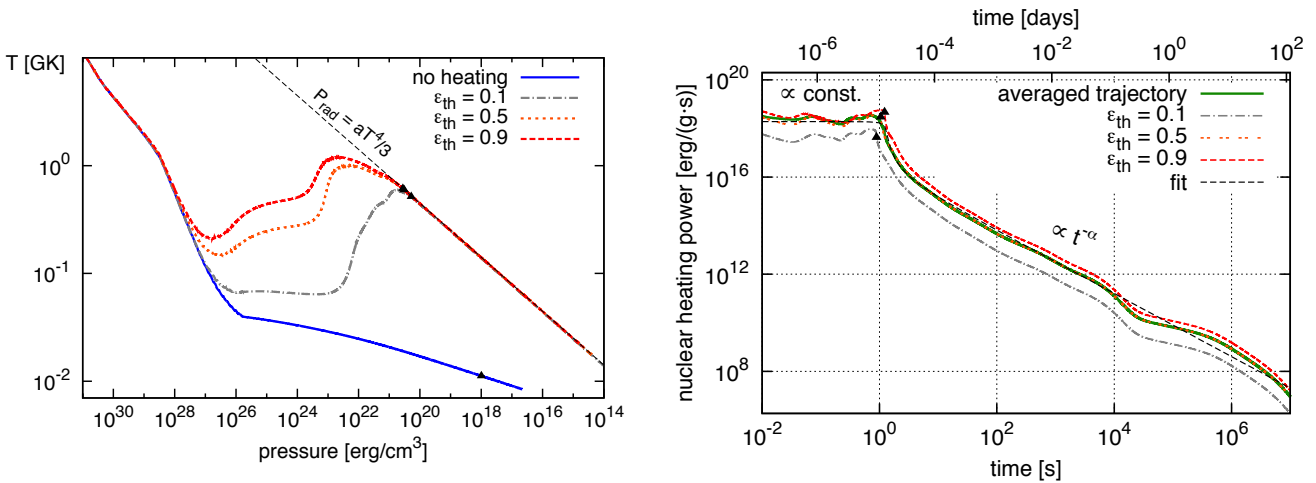


Figure 7. Left: postprocessed temperature as a function of pressure for the cases without nuclear heating (dashed line) and with heating efficiencies $\epsilon_{th} = 0.1, 0.5$ and 0.9 . Right: nuclear heating power as a function of time, along with a power-law fit $\propto t^{-\alpha}$ with index $\alpha = 1.3$. The small black triangles on each trajectory are neutron freeze-out points (the points in which $Y_n/Y_{seed} = 1$).

are the nuclear masses, which determine the location of the drip line and the evolution of the path, and the fission barriers and yields distribution, which are responsible for the abundances between $120 < A < 170$. We explicitly explore how sensitive our results are to the details of our nuclear physics input. In Fig. 6, left panel, we show the effect of including heating with different efficiencies of the profile of final abundances. In all cases the second and third r-process peak are robustly reproduced, but the regions behind the peaks are less populated if heating is included. In the middle panel we vary the fraction of nuclear energy that is retained in the matter, ϵ_{th} . As long as ϵ_{th} is above some threshold value ($\sim 1\%$) the resulting abundances are independent of the exact choice. In the right panel we explore the sensitivity to the fission prescription. We once follow Panov et al. (2001) assuming only two fission daughter nuclei and, alter-

natively, we adopt the fission treatment and yield distribution of Kodama & Takahashi (1975). When using the latter, the trough after the second peak completely fills up while for the Panov prescription the fission products end up entirely in the second peak. Note that the used prescription of Panov uses only two daughter nuclei while he also provides yield distributions in a more recent paper (Panov et al. 2008). Therefore the deviation of our results from the solar system abundances are sensitive to the physics of extremely neutron-rich nuclei.

In Fig. 7, left panel, we show the evolution of a trajectory in the pressure-temperature plane for different heating efficiencies, the right panel shows the generated nuclear power. The early evolution is very similar for all four cases because the internal energy is high and the contribution from the generated heat is negligible. The latter becomes the domi-

nant part of the internal energy after about 20 ms when the temperature and density decrease enough for *r*-process to begin. Similar to Freiburghaus et al. (1999) we find that the generated nuclear energy raises the temperature by almost an order of magnitude compared to the case without heating. Matter essentially stays in (n, γ) - (γ, n) equilibrium until the neutron-to-seed ratio drops below unity (“freeze-out”). Note that all non-zero heating efficiencies produce trajectories that lie on the $P = 1/3aT^4$ -line at freeze-out and therefore follow a similar behaviour in their decay to stability. The reason is that for our extremely neutron-rich conditions the main contribution to the pressure comes from neutrons and photons, while the electron pressure is orders of magnitude smaller. Therefore, at the freeze-out point when most of the neutrons are captured the system is radiation pressure dominated³.

Later the system evolution enters the radiation-dominated expansion which was studied in Li & Paczyński (1998). In this regime the generated nuclear heat comes mainly from β -decays and can overall be well approximated by a power law, while before the freeze-out the generated heat stays approximately constant (see Fig. 7). We suggest the following fit which smoothly interpolates between a constant value and a power law:

$$\dot{\epsilon}(t) = \epsilon_0 \left(\frac{1}{2} - \frac{1}{\pi} \arctan \frac{t - t_0}{\sigma} \right)^\alpha \times \left(\frac{\epsilon_{th}}{0.5} \right) \quad (4)$$

with $\epsilon_0 = 2 \times 10^{18}$ erg/(g s), $t_0 = 1.3$ s, $\sigma = 0.11$ s, and $\alpha = 1.3$. This formula yields a good fit to all heating histories. Similarly to the trajectory considered in Metzger et al. (2010), in our case starting from ~ 10 s the nuclear heating power becomes essentially independent from the initial conditions. The deviations from a power law that are visible in the right panel of Fig. 7 at $t \sim 10^{-1}$ d and $t \sim 20$ d are due to the decay of individual elements.

To explore the dependence of the final abundances on the electron fraction Y_e , we show in Fig. 8 the resulting abundances for some of the few trajectories with higher Y_e -values (colour; for comparison the results from the dominating low- Y_e trajectories are shown in gray). For Y_e up to ~ 0.15 the results hardly deviate from each other, only at and above this value do the abundances below $A \sim 110$ start to deviate. Substantial deviations for the abundance pattern of the heaviest nuclei with $A > 110$ only occur for $Y_e > 0.2$, since here the Y_e increase is triggered by shocks at low density, the neutron density drops earlier and the neutron captures freeze out.

4 SUMMARY AND DISCUSSION

In this study we have re-examined the question of heavy element nucleosynthesis in compact binary mergers. Our study adds several new aspects in comparison with earlier work. First, we systematically cover the plausible ns^2 parameter space with masses from 1.0 to 2.0 M_\odot in 21 simulations. Despite the long history of ns^2 simulations we

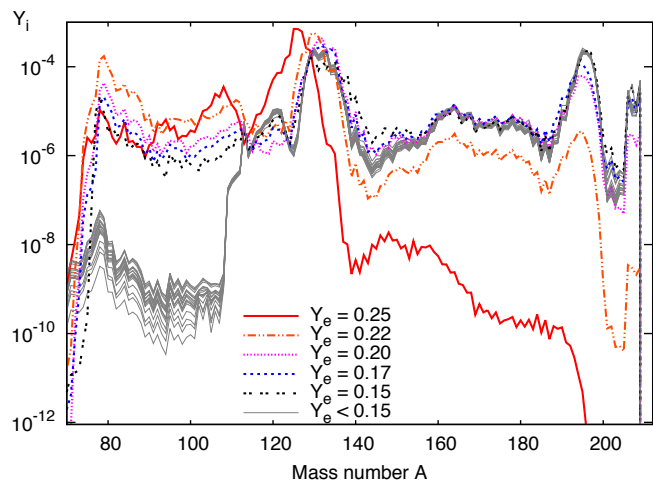


Figure 8. Dependence of the final abundances on the electron fraction. Shown are the final abundances of some trajectories with high Y_e (in colour), they are compared to the low- Y_e trajectories (gray) that dominate the ejecta. Below $Y_e = 0.1$ two or more fission cycles occur, one or two are realized for $0.1 < Y_e < 0.22$ and none for $Y_e > 0.22$. Since high- Y_e trajectories only represent a very small mass fraction, their contribution to the overall abundances is minuscule.

are not aware of any study that has systematically explored such a wide range of ns masses. We complement these cases with mergers of a 1.4 M_\odot neutron star with black holes of 5 and 10 M_\odot . Second, since we use a nuclear equation of state with neutron stars in initial cold β -equilibrium and include Y_e -changing weak interactions, we overcome the Y_e -ambiguity that has plagued all previous studies. We subsequently find the final abundances by following the nucleosynthesis along a large set of hydrodynamic trajectories with a state-of-the-art nuclear reaction network.

Consistent with earlier studies, we find a very robust *r*-process and final abundances that are in good agreement with the heavy solar system abundance pattern. The major new result is that the final pattern is extremely robust across the whole parameter space: all 21 ns^2 -merger and the two $nsbh$ -merger cases yield practically identical nucleosynthesis outcomes. The major reason for this unique abundance pattern is the extreme neutron richness of the ejecta, $\langle Y_e \rangle \approx 0.04$. Consequently, in each case the *r*-process path meanders along the neutron drip line and matter undergoes several fission cycles, so that the abundances are determined entirely by nuclear rather than by astrophysical properties. As a corollary, the poorly known nuclear properties near the neutron dripline do have an impact on the resulting abundance pattern. We find some dependence on the used mass formula and on the distribution of the nuclear fragments after fissioning. Nevertheless, the second and third *r*-process peaks are robustly reproduced, without any “tuning” of the nuclear physics input the overall agreement with the solar system *r*-process pattern is good. *R*-process matter lighter than $\sim A \approx 120$, however, is substantially under-produced with respect to the solar system pattern. The few high- Y_e trajectories produce different abundance patterns, see Fig. 8, but there is too little mass in this

³ At higher temperatures the radiation pressure must necessarily include contribution from electron-positron pairs (Witti et al. 1994; Farouqi et al. 2010).

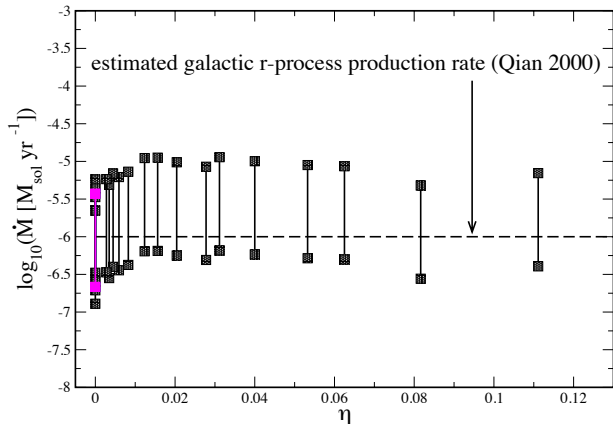


Figure 9. Relevance of the ejected mass for the r-process enrichment of the galaxy. The mass asymmetry parameter η , see Eq. (1), is used here to label the different simulations. Adopting the 95% confidence interval for the galactic double neutron star merger rate from (Kalogera et al. 2004), we calculate which galactic enrichment rates would result for the ejected matter of our simulations (lines with squares at ends; our reference case of two $1.4 M_{\odot}$ neutron stars is shown in magenta). For comparison we also plot the estimated galactic enrichment rate (Qian 2000). All the ejected masses are consistent with being a major contributor to galactic r-process, even if the total amount per event should be decreased by a factor of a few (say, due to equation of state or GR effects).

material to leave a noticeable impact in the resulting average distribution.

One may wonder whether captures of neutrinos from the central remnant, which are not included in our simulations, could change the Y_e of the ejecta noticeably. For two reasons, we do not think that this is the case. First, the ejecta are launched practically at first contact, see Fig. 2, with $\langle v \rangle > 0.1c$, (Piran et al. 2012). The neutrino emission, however, only becomes relevant after a disk has formed which takes ~ 7 more milliseconds (e.g. Fig. 7 in Rosswog et al. (2012)) at which time the solid angle under which the escaping matter is seen has decreased already by a large factor. Second, the ejecta are concentrated in the orbital plane while the neutrinos are emitted preferentially perpendicular to it, see Fig. 12 in Rosswog & Liebendörfer (2003) and Fig. 9 in Dessart et al. (2009). We therefore expect Y_e -changes due to neutrino captures to be negligible⁴.

The dynamic ejecta masses are large enough to make a substantial contribution to the chemical enrichment of the galaxy with r-process material. Adopting the observation-based double neutron star merger rates of Kalogera et al. (2004), $R_{\text{DNS}} = 83.0_{-66.1}^{+209.1} \text{ yr}^{-1}$, we calculate by which average rate the galaxy would be r-process enriched from neutron star mergers. Although the overall ejecta masses vary by more than a factor of five between different cases, all

of them are perfectly consistent with the estimated galactic enrichment rate (Qian 2000), see Fig. 9. The reference case of $2 \times 1.4 M_{\odot}$ neutron stars (shown in magenta), nicely brackets this value. This also implies that the relevance of compact binary mergers for r-process remains unaffected even if the typical ejecta amount per event should be decreased by a factor of a few, say, due to equation of state or GR effects.

Our findings of ejecta masses in the required range, extremely robust abundance patterns for the heaviest r-process elements, but underproduction of the lighter r-process elements, make compact binary mergers the major candidate for the observed, unique, heavy r-process component (Snedden et al. 2008). At the same time this means, that at least one, but possibly more additional r-process sites must contribute to the cosmic chemical evolution of lighter r-process elements.

An important question is how early the r-process yields from compact binary mergers would be available for cosmic enrichment. The inspiral time from the birth of a compact binary system to a coalescence is very sensitive to both the initial separation and the orbital eccentricity (Peters & Mathews 1963, 1964). The initial separation is set by binary evolution processes which are beyond the scope of this paper, but it is worth re-iterating that a binary system that survives the two SN explosions that are required to form the system in the first place will in most cases possess a large orbital eccentricity. As illustrated in Fig. 10 short lifetimes can be achieved with plausible orbital parameters. For example, an initial semi-major axis of $1 R_{\odot}$ and an eccentricity of 0.9 lead to a merger only 1 Myr after binary formation (for comparison we note that the projected semi-major axis of the double pulsar PSR J0737-3039 A+B (Burgay et al. 2003; Kramer & Stairs 2008) is $0.6 R_{\odot}$). Some binary population synthesis studies (Dewi & Pols 2003; Belczynski et al. 2006) find indeed short-lived channels that coalesce essentially *at birth*, so an early enrichment from compact mergers is at least plausible. Earlier studies (Argast et al. 2004) disfavoured neutron star mergers as dominant galactic r-process source. Based on our hydrodynamic plus nucleosynthesis studies, however, we have shown that compact binary mergers are excellent production sites for the unique, heavy r-process component. We leave the question of whether or to which extent they are consistent with cosmic chemical evolution for future studies.

ACKNOWLEDGMENTS

This work was supported by DFG grant RO-3399, AOBJ-584282. S.R. thanks Enrico Ramirez-Ruiz/UC Santa Cruz and Andrew MacFadyen/NYU for their hospitality and for many stimulating conversations. We also thank Gabriel Martinez-Pinedo for useful discussions on r-process nucleosynthesis. Our particular thanks goes to K.-L. Kratz and F.-K. Thielemann for their continued support and interest in our work. Especially FKT has educated us on this exciting topic and we are grateful for his insightful comments on an earlier version of this manuscript. We acknowledge the use of the visualization software SPLASH developed by Daniel Price (2007). The simulations of this paper were performed

⁴ This may be different for likely emerging neutrino-driven winds that might also contribute to the nucleosynthesis of compact binary merger events.

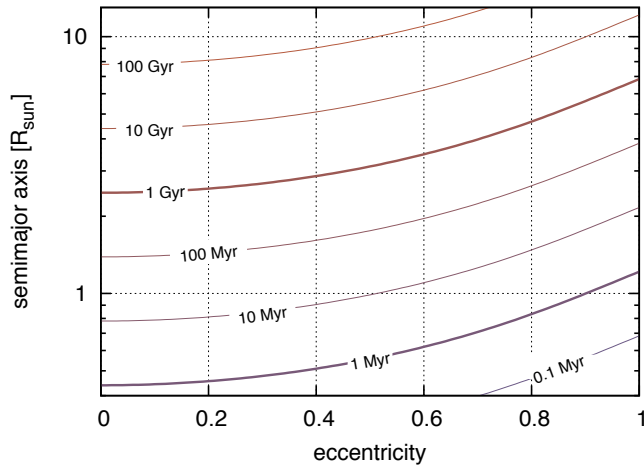


Figure 10. Contour plot of the estimated lifetimes of a $1.4\text{-}1.4 M_{\odot}$ binary for different orbital eccentricities and semimajor axes (Peters & Mathews 1964).

on the facilities of the Höchstleistungsrechenzentrum Nord (HLRN). A. A. is supported by the Helmholtz-University Young Investigator Grant No. VH-NG-825.

REFERENCES

- Abadie J., Abbott B. P., Abbott R., Abernathy M., Accadia T., Acernese F., Adams C., Adhikari R., Ajith P., Allen B., et al. 2010, *Classical and Quantum Gravity*, 27, 173001
- Abbott B. P., Abbott R., Adhikari R., Ajith P., Allen B., Allen G., Amin R. S., Anderson S. B., Anderson W. G., Arain M. A., et al. 2009, *Reports on Progress in Physics*, 72, 076901
- Arcones A., Janka H.-T., Scheck L., 2007, *A & A*, 467, 1227
- Arcones A., Martinez-Pinedo G., 2011, *Phys. Rev. C*, 83, 045809
- Arcones A., Montes F., 2011, *ApJ*, 731, 5
- Argast D., Samland M., Thielemann F.-K., Qian Y.-Z., 2004, *A&A*, 416, 997
- Belczynski K., Perna R., Bulik T., Kalogera V., Ivanova N., Lamb D. Q., 2006, *ApJ*, 648, 1110
- Bildsten L., Cutler C., 1992, *ApJ*, 400, 175
- Burbidge G., Burbidge R., Fowler W., Hoyle F., 1957, *Rev. Mod. Phys.*, 29, 547
- Burgay M., D’Amico N., Possenti A., Manchester R. N., Lyne A. G., Joshi B. C., McLaughlin M. A., Kramer M., Sarkissian J. M., Camilo F., Kalogera V., Kim C., Lorimer D. R., 2003, *Nature*, 426, 531
- Cowan J. J., Sneden C., 2006, *Nature*, 440, 1151
- Demorest P. B., Pennucci T., Ransom S. M., Roberts M. S. E., Hessels J. W. T., 2010, *Nature*, 467, 1081
- Dessart L., Ott C. D., Burrows A., Rosswog S., Livne E., 2009, *ApJ*, 690, 1681
- Dewi J. D. M., Pols O. R., 2003, *MNRAS*, 344, 629
- Eichler D., Livio M., Piran T., Schramm D. N., 1989, *Nature*, 340, 126
- Farouqi K., Kratz K.-L., Pfeiffer B., Rauscher T., Thielemann F.-K., Truran J. W., 2010, *ApJ*, 712, 1359
- Fischer T., Whitehouse S. C., Mezzacappa A., Thielemann F.-K., Liebendörfer M., 2010, *A & A*, 517, A80
- Fitchett M. J., 1983, *MNRAS*, 203, 1049
- Freiburghaus C., Rosswog S., Thielemann F.-K., 1999, *ApJ*, 525, L121
- Frischknecht U., Hirschi R., Thielemann F.-K., 2012, *A & A*, 538, L2
- González J. A., Hannam M., Sperhake U., Brüggmann B., Husa S., 2007, *Physical Review Letters*, 98, 231101
- Goriely S., Bauswein A., Janka H.-T., 2011, *ApJL*, 738, L32
- Honda S., Aoki W., Ishimaru Y., Wanajo S., Ryan S. G., 2006, *ApJ*, 643, 1180
- Hüdepohl L., Müller B., Janka H.-T., Marek A., Raffelt G. G., 2010, *Physical Review Letters*, 104, 251101
- Kalogera V., Kim C., Lorimer D. R., Burgay M., D’Amico N., Possenti A., Manchester R. N., Lyne A. G., Joshi B. C., McLaughlin M. A., Kramer M., Sarkissian J. M., Camilo F., 2004, *ApJL*, 614, L137
- Kiziltan B., Kottas A., Thorsett S. E., 2010, *ArXiv e-prints*
- Kochanek C., 1992, *ApJ*, 398, 234
- Kodama T., Takahashi K., 1975, *Nuclear Physics A*, 239, 489
- Kramer M., Stairs I. H., 2008, *Annual Review of Astronomy and Astrophysics*, 46, 541
- Kulkarni S. R., 2005, *ArXiv Astrophysics e-prints*
- Lattimer J. M., Prakash M., 2010, *ArXiv e-prints*
- Lattimer J. M., Schramm D. N., 1974, *ApJ*, (Letters), 192, L145
- Lattimer J. M., Schramm D. N., 1976, *ApJ*, 210, 549
- Li L., Paczyński B., 1998, *ApJL*, 507, L59
- Metzger B. D., Arcones A., Quataert E., Martinez-Pinedo G., 2010, *MNRAS*, 402, 2771
- Metzger B. D., Berger E., 2012, *ApJ*, 746, 48
- Metzger B. D., Martinez-Pinedo G., Darbha S., Quataert E., Arcones A., Kasen D., Thomas R., Nugent P., Panov I. V., Zinner N. T., 2010, *MNRAS*, 406, 2650
- Möller P., Nix J. R., Myers W. D., Swiatecki W. J., 1995, *At. Data Nucl. Data Tables*, 59, 185
- Monaghan J. J., 2005, *Reports on Progress in Physics*, 68, 1703
- Nakar E., Piran T., 2011, *Nature*, 478, 82
- Oechslin R., Janka H., Marek A., 2007, *A & A*, 467, 395
- Panov I. V., Freiburghaus C., Thielemann F.-K., 2001, *Nuclear Physics A*, 688, 587
- Panov I. V., Korneev I. Y., Rauscher T., Martinez-Pinedo G., Kelić-Heil A., Zinner N. T., Thielemann F.-K., 2010, *A & A*, 513, A61
- Panov I. V., Korneev I. Y., Thielemann F.-K., 2008, *Astronomy Letters*, 34, 189
- Peters P., Mathews J., 1963, *Phys. Review*, 131, 435
- Peters P., Mathews J., 1964, *Phys. Review*, B136, 1224
- Piran T., Nakar E., Rosswog S., 2012, e-print arXiv:1204.6242
- Podsiadlowski P., Langer N., Poelarends A. J. T., Rappaport S., Heger A., Pfahl E., 2004, *ApJ*, 612, 1044
- Price D. J., 2007, *Publications of the Astronomical Society of Australia*, 24, 159
- Qian Y.-Z., 2000, *ApJL*, 534, L67
- Rauscher T., Thielemann F.-K., 2000, *Atomic Data and*

- Nuclear Data Tables, 75, 1
- Roberts L. F., Kasen D., Lee W. H., Ramirez-Ruiz E., 2011, *ApJL*, 736, L21+
- Roberts L. F., Woosley S. E., Hoffman R. D., 2010, *ApJ*, 722, 954
- Rosswog S., 2005, *ApJ*, 634, 1202
- Rosswog S., 2009, *New Astronomy Reviews*, 53, 78
- Rosswog S., Davies M. B., 2002, *MNRAS*, 334, 481
- Rosswog S., Davies M. B., Thielemann F.-K., Piran T., 2000, *A&A*, 360, 171
- Rosswog S., Liebendörfer M., 2003, *MNRAS*, 342, 673
- Rosswog S., Liebendörfer M., Thielemann F.-K., Davies M., Benz W., Piran T., 1999, *A & A*, 341, 499
- Rosswog S., Piran T., Nakar E., 2012, e-print arXiv:1204.6240
- Rosswog S., Ramirez-Ruiz E., Davies M. B., 2003, *MNRAS*, 345, 1077
- Rosswog S., Ramirez-Ruiz E., Hix W. R., Dan M., 2008, *Computer Physics Communications*, 179, 184
- Schwab J., Podsiadlowski P., Rappaport S., 2010, *ApJ*, 719, 722
- Sengupta A. S., LIGO Scientific Collaboration Virgo Collaboration 2010, *Journal of Physics Conference Series*, 228, 012002
- Shen H., Toki H., Oyamatsu K., Sumiyoshi K., 1998a, *Nuclear Physics, A* 637, 435
- Shen H., Toki H., Oyamatsu K., Sumiyoshi K., 1998b, *Progress of Theoretical Physics*, 100, 1013
- Smith J. R., 2009, *Classical and Quantum Gravity*, 26, 114013
- Snedden C., Cowan J. J., Gallino R., 2008, *Annual Review of Astronomy and Astrophysics*, 46, 241
- Thielemann F.-K., Arcones A., Käppeli R., Liebendörfer M., Rauscher T., Winteler C., Fröhlich C., Dillmann I., Fischer T., Martinez-Pinedo G., Langanke K., Farouqi K., Kratz K.-L., Panov I., Korneev I. K., 2011, *Progress in Particle and Nuclear Physics*, 66, 346
- Thorsett S., Chakrabarti D., 1999, *ApJ*, 7512, 288
- Timmes F. X., Swesty F. D., 2000, *ApJS*, 126, 501
- Valentim R., Rangel E., Horvath J. E., 2011, *MNRAS*, p. 409
- van den Heuvel E. P. J., 2004, in V. Schoenfelder, G. Lichti, & C. Winkler ed., 5th INTEGRAL Workshop on the INTEGRAL Universe Vol. 552 of ESA Special Publication, X-Ray Binaries and Their Descendants: Binary Radio Pulsars; Evidence for Three Classes of Neutron Stars?. p. 185
- van Kerkwijk M. H., Breton R. P., Kulkarni S. R., 2011, *ApJ*, 728, 95
- Wanajo S., Janka H.-T., 2012, *ApJ*, 746, 180
- Winteler C., 2012, PhD thesis, University Basel, CH
- Winteler C., Käppeli R., Perego A., Arcones A., Vasset N., Nishimura N., Liebendörfer M., Thielemann F.-K., 2012, *ApJL*, 750, L22
- Witti J., Janka H.-T., Takahashi K., 1994, *A&A*, 286, 841